J Solid State Electrochem (2002) 6: 111–118
DOI 10.1007/s100080100200

ORIGINAL PAPER

C.M.V.B. Almeida · B.F. Giannetti

Comparative study of electrochemical and thermal oxidation of pyrite

Received: 28 March 2000 / Accepted: 2 February 2001 / Published online: 16 October 2001

Abstract The oxidation of pyrite was studied as a function of grain size, employing voltammetric and thermal analysis. The data obtained with the electrochemical experiments are consistent with the results shown in the thermogravimetry-differential thermogravimetry (TG-DTG) records. The use of both techniques revealed that oxidation of the mineral is affected by the grain size employed. The maximum yield of SO_4^{2-} was obtained from electrodes constructed with <210 μm-sized particles. The same behavior was observed during thermal decomposition. When the temperature surpasses 490 °C, the small particles (<210 μm) oxidize in a single step which is not affected by changes in the rate of air flow, indicative of their higher reactivity among the ground mineral electrodes. The comparison between the results obtained by the two methods suggests that, below 490 °C or 0.6 V, pyrite oxidation, either in air or in aqueous media, is similar and depends on the semiconducting properties of the mineral.

Keywords Voltammetry · Thermal analysis · Pyrite particles · Electrochemical dissolution · Surface reactivity

Introduction

Minerals respond to the environment through their surface. The physical and chemical properties of the surfaces play an important role in metal deposit formation and in hydrometallurgical processes. The redox reactivity of iron sulfides, in addition to their abundance, accounts for the variety of geochemical processes in which they are involved. Hence, it is highly desirable to obtain some information on the reactivity of the mineral surfaces before the leaching and flotation processes take place.

Fracturing and grinding are common processes applied to rocks and ores to separate phases of economic interest and to characterize analytically the materials. The efficiency of the flotation and leaching processes and the mineral solubility will depend on the physical and chemical conditions of the surfaces, which restricts the reactivity between the solid and liquid phases. One of the customary methods of determining the surface reactivity of minerals is the evaluation of their dissolution rate by quantifying the content of a dissolved substance in a proper medium [1]. However, this is a quite slow and labor-consuming method.

In the present work, measurements of the anodic dissolution current of carbon paste electrodes were compared with the results of thermal analysis. Carbon paste electrodes have already been applied to the study of electrochemical dissolution processes of different powder and granulate materials [2, 3, 4]. The use of cyclic voltammetry allows estimation of the relative quantity of oxidation products produced during the mineral dissolution. On the other hand, thermal analysis may be used as a tool to assist in the study of the electrochemical behavior of the mineral. This technique permits the evaluation of the surface condition when in contact with air and the oxidation process in the absence of a liquid phase.

The aim of this work is to compare the results obtained by electrochemical and thermal methods regarding the grain size of the samples.

Experimental

The ore pyrite samples investigated were from Morro Velho Mine, in Nova Lima, Minas Gerais, Brazil. A quantity of the mineral was hand ground in an agate mortar and pestle. This material was then sieved to isolate the fractions containing particles <210 μm, 210–250 μm and >250 μm in size. The three electrodes were designated Py21, Py2125 and Py25, respectively.

C.M.V.B. Almeida · B.F. Giannetti (✉)
LaFTA – Laboratório de Físico-Química Teórica e Aplicada, Instituto de Ciências Exatas e Tecnologia da Universidade Paulista, R. Dr. Bacelar 1212, Cep 04026-002, São Paulo, Brazil
E-mail: biafgian@unip.br

Potentiodynamic measurements were carried out in a standard electrochemical cell. A selected crystal of pyrite was cut to size and mounted in polyester resin with one surface exposed. This electrode was used to compare the data obtained with others found in the literature [3, 5]. The exposed surface was polished wet on 600-grit silicon carbide paper, washed with triply distilled water and transferred quickly to the cell. The carbon paste electrodes consisted of 1.0 g graphite and 1.2 g paraffin wax (solidification point 68–74 °C) containing 5 mg of ground mineral. For the construction of the carbon paste electrodes, 5.0 mg of ground mineral was placed in a Teflon cavity of diameter 4.5 mm. Then, a brass wire of diameter 3.0 mm was immersed in the graphite/paraffin mixture heated at 70 °C. The extremity of the wire covered with the hot mixture was immediately pressed on the pyrite particles placed in the mould. The resulting set is a pyrite disk with diameter nearly 4.0 mm, which covers the graphite surface almost completely. The lateral parts of the electrode were then covered with Teflon tape to avoid contact with solution. Figure 1 shows SEM micrographs of the crystal sample (geometric area of 15 mm^2) and of the Py21 carbon paste electrode fixed as described above. It can be seen that the graphite/paraffin mixture exposed to the solution is minimal. The area of the ground electrodes can be roughly estimated (see Fig. 1). The geometric area of the polished electrode shown by the micrograph can be estimated as about 0.95 mm^2. In the same area it is possible to place 15 pyrite particles of 210 μm in size. Considering the exposed particles as half cubes, the area in the micrograph of the Py21 electrode can be calculated as 1.9 mm^2. Despite the simplicity of the model employing geometric areas, it is clear that the area of the ground electrodes is larger than that of the polished ones, even without taking into account the roughness of each particle.

The reference electrode was an Ag/AgCl electrode placed in a Luggin-Haber capillary and the counter electrode was a platinized platinum wire of large area. The electrolyte buffer, acetic acid/sodium acetate, pH 4.5, was prepared from Merck p.a. grade reagent and triply distilled water. Nitrogen was bubbled through the cell to deaerate the solution. Potentials values quoted in this text are given on the standard hydrogen electrode (SHE) scale. All experiments were carried out at 25 °C at a scan rate of 20 mV s^{-1}.

Thermogravimetry-differential thermogravimetry (TG-DTG) measurements were performed using a Shimadzu thermal analyzer. Approximately 5 mg of the sample was weighed into a platinum crucible, spread as far as possible as a monolayer and placed in the TG-DTG apparatus. The heating rate was established at 10 °C min^{-1}. The temperature program was started at room temperature and completed at 900 °C. The pyrite sample was oxidized under a variety of experimental conditions. The sets of experiments involved changing the gas flow between 10 and 80 mL min^{-1} and changing the particle size between 210 and 250 μm. To establish the reaction sequences, the reactions were stopped at 550 °C and 900 °C and phase analysis was performed using infrared spectroscopy.

Results and discussion

Electrochemical behavior

Cyclic voltammetric measurements were used in the present experiments in order to obtain basic information concerning the FeS_2 dissolution. The reverse process, the reduction of the oxidation products, was also examined.

Figure 2 shows the anodic *E-I* curves of pyrite in acetic acid/sodium acetate buffer. The anodic oxidation in the positive-going scan initiates at similar potentials for all electrodes and a higher current was observed for the polished electrode. In the curves of the electrodes constructed with the ground mineral, a current peak designated A_1 arises. This current is also observed on the massive specimen curves, but only during the second cycle. The carbon paste electrodes are not polished and

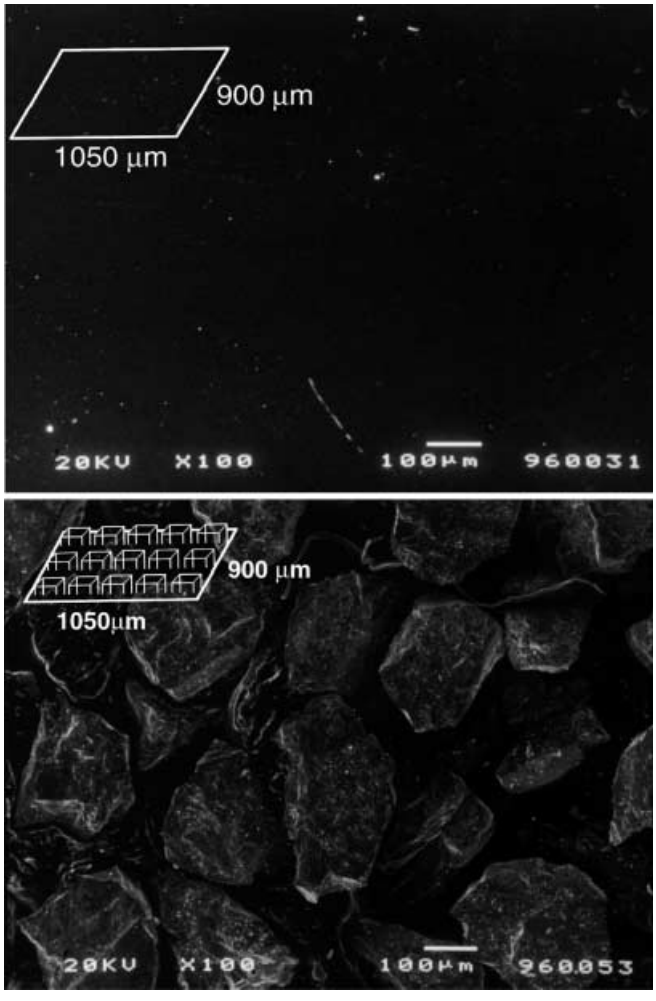

Fig. 1 SEM micrographs of pyrite electrode surfaces. Polished (*top*) and Py21 ground electrode (*bottom*)

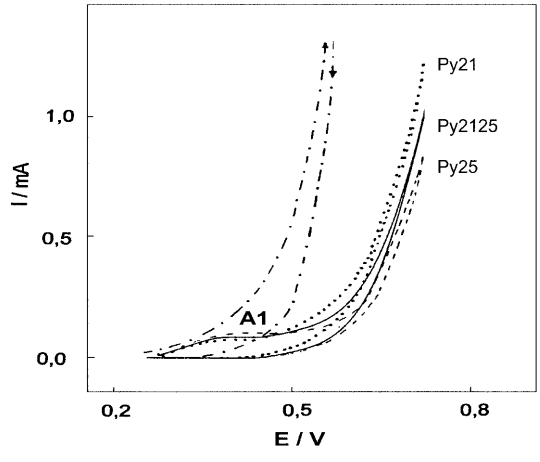

Fig. 2 Anodic curves of pyrite in acetic acid/acetate buffer, pH 4.5, at 298 K and sweep rate 20 mV s^{-1}: (· · ·) Py21, (- -) Py2125, (- - -) Py25 and (- · -) polished electrode

pyrite particles may be partially covered by iron hydroxides/oxides formed in air during grinding. Preparation, grinding and prolonged oxidation of pyrite in air should produce mainly a basic iron sulfate similar to jarosite and iron oxide/hydroxide [6]. However, the increased surface roughness due to the preparation seems to favor the formation of iron oxide/hydroxide over sulfate, in contrast to the natural weathering process of pyrite [6, 7, 8, 9].

It can clearly be seen that with increasing particle size the relative anodic current decreases, possibly owing to the change in surface area. The results in Fig. 2 show further that ground particle electrodes, even with a larger area, present smaller anodic currents than those that were mechanically polished.

The anodic reactions of pyrite are fairly well discussed in the literature [5, 10, 11] and may be represented, briefly, by the reactions 1, 2, 3:

$$FeS_2 \rightarrow Fe^{2+} + 2S + 2e^- \quad (1)$$

$$FeS_2 + 8H_2O \rightarrow Fe^{2+} + 2SO_4^{2-} + 16H^+ + 14e^- \quad (2)$$

$$Fe^{2+} \rightarrow Fe^{3+} + e^- \quad (3)$$

Figure 3 shows that the oxidation/reduction process is irreversible in the electrochemical sense: the total anodic charge (Q_a) is greater than the total cathodic charge (Q_c). In the curves of the electrodes constructed with ground mineral, peak A_1 arises at nearly 0.45 V, suggesting that Fe(II) species are oxidized in this potential range [5, 6, 7, 8, 9, 10, 11]. The association of Nernstian potentials with current peaks is common in the literature. However, this approach may bring doubts when irreversible processes are studied.

In order to confirm whether peak A_1 results from the oxidation of iron oxides/hydroxides present on the electrode surface, voltammograms were recorded in the potential region of –0.08 V to 0.7 V (Fig. 4). The cyclic voltammogram obtained from a carbon paste electrode without any preparation is shown in Fig. 4 as a dashed line. The reduction charge is almost equal to the oxidation charge for one cycle, providing further evidence to support the possibility of a reversible oxidation-reduction process. This is in agreement with voltammetric studies of iron oxides in acidic medium [12, 13, 14].

Figure 4 also shows that adding Fe^{2+} (sulfate) to the solution increases peaks A_1 and C_1 (continuous line). Thus, the anodic peak A_1 at 0.45 V was associated with reaction 4 and the cathodic peak C_1, recorded during the reverse scan at 0.25 V, was related to the reaction:

$$Fe^{2+} + 3H_2O \rightarrow Fe(OH)_3 + 3H^+ + e^- \quad (4)$$

As the scan is taken more negative values, current peak C_2 appears (Fig. 3). This current peak has been attributed to the reduction of sulfur, $E_T = -0.04$ V [7, 8, 9, 10, 11], formed during the anodic scan as represented in reaction 5:

$$S + 2H^+ + 2e^- \rightarrow H_2S \quad (5)$$

In order to quantify the oxidation products formed, the charge passed in the anodic and cathodic processes was determined by integration of the area under the voltammograms, on the positive-going and subsequent return scans, at 20 mV s^{-1}. It was assumed that the charge passed in the anodic process is determined by the area under the voltammogram, at 20 mV s^{-1}, and is related to reactions 1, 2, 3. Thus the total anodic area is given by $Q_a = (3x + 15y)$ F, where x and y are the number of moles of pyrite oxidized. As current peak C_2 was related to S reduction, the charge passed equals 4 F since the oxidation of pyrite by reaction 1 produces two atoms of sulfur. The cathodic current peak C_1 was related to the $Fe(OH)_3$ reduction, being $Q_{C1} = 15$ F, the charge consumed in the process. The difference between Q_a and Q_c is caused by the soluble species formed, SO_4^{2-}, during oxidation. The sulfate formed diffuses into solution [5] and its reduction does not occur in the

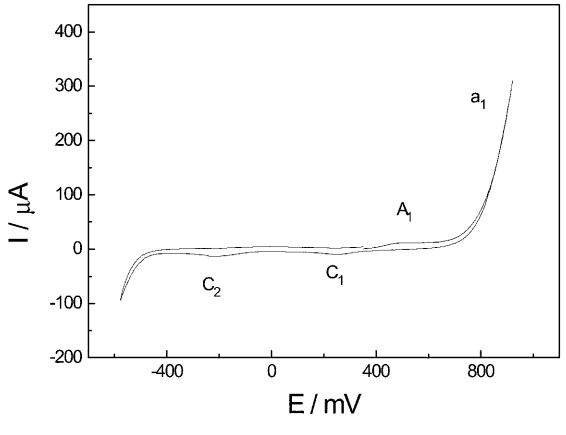

Fig. 3 Cyclic voltammogram of Py21 in acetic acid/acetate buffer, pH 4.5, at 298 K and sweep rate 20 mV s^{-1}

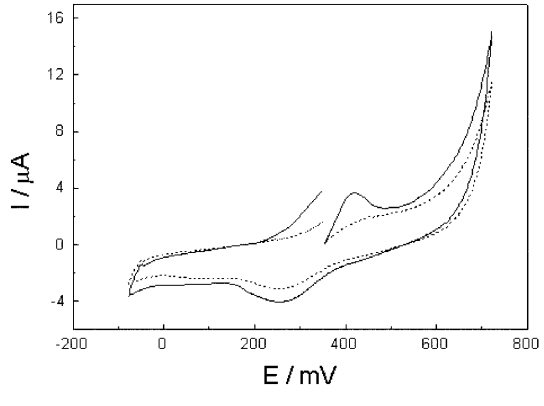

Fig. 4 Cyclic voltammograms of pyrite, at 298 K and sweep rate 20 mV s^{-1}, in the potential range between –0.522 V and 0.7 V: (- - -) in acetic acid/acetate buffer, pH 4.5, and (—) in acetic acid/acetate buffer plus 10^{-3} M $FeSO_4$

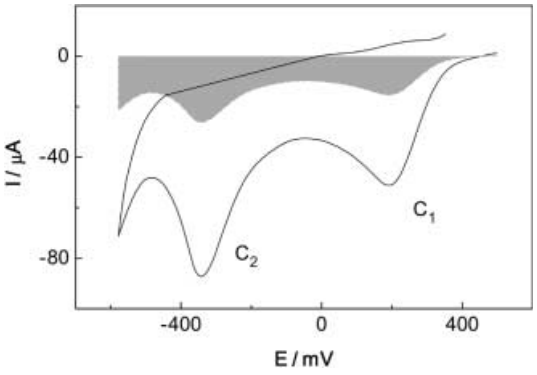

Fig. 5 Detail of the cathodic segment of the voltammogram of Py21 in acetic acid/acetate buffer performed on the positive-going scan, $E_{\lambda a} = 0.8$ V, pH 4.5, at 298 K and sweep rate 20 mV s^{-1}, $E_i = E_{oc}$. The gray area represents the charge corresponding to pyrite decomposition discounted when a negative-going scan is performed, $E_i = E_{oc}$ and $E_i = E_{\lambda c}$

potential range of this study [15]. Thus, the quantity of SO_4^{2-} formed during oxidation may be evaluated from the difference between the total anodic and cathodic charges. The cathodic charge associated with the reduction of $Fe(OH)_3$ was estimated in the potential range between 0.35 V and 0.05 V (Q_{c1}). The charge due to reaction 5 was obtained between 0.0 V and –0.4 V (Q_{c2}). As the charge values so obtained include the contribution of pyrite decomposition (reaction 6), the value of the charge obtained on the negative-going scan, beginning at the open circuit potential, was subtracted over this potential range (Fig. 5):

$$FeS_2 + 2H^+ + 2e^- \rightarrow FeS + H_2S \quad (6)$$

The area of the carbon paste electrodes is unknown. Thus, to evaluate the quantities of SO_4^{2-}, S and $Fe(OH)_3$ produced by the electrodes, relative quantities of soluble compounds, iron(III) hydroxide and elemental sulfur were calculated as shown in Table 1.

Figure 6 shows the variation of the Q_a/Q_c ratio with the anodic end point potential, $E_{\lambda a}$, for the four electrodes. The dissolution of the polished surface is more intense than that observed when ground mineral is used. The relative quantity of the oxidation products changes with the particle size and with the reactivity of the surface. This result corresponds with other studies on pyrite leaching [15, 16, 17], where it was observed that the dissolution rate changes with the particle size.

The relative quantity of iron hydroxide is independent of $E_{\lambda a}$ for the polished electrode. However, the ground electrodes show a decrease of the percentage of $Fe(OH)_3$ on increasing the potential (Fig. 7a). This difference may be attributed to the iron hydroxides that are present on the surface before oxidation (Fig. 2) and may delay the sulfate production.

Figure 7b shows the variation of the percentage of SO_4^{2-} as a function of the anodic end point potential. The SO_4^{2-} yield increases as the grain size decreases. At potentials more negative than 0.6 V the sulfate produced

Table 1 Evaluation of the relative quantities of the oxidation products of pyrite

% SO_4^{2-}	$[(Q_a - Q_c)/Q_a] \times 100$
% $Fe(OH)_3$	$(Q_{c1} - Q_a) \times 100$
% S	$(Q_{c2} - Q_a) \times 100$

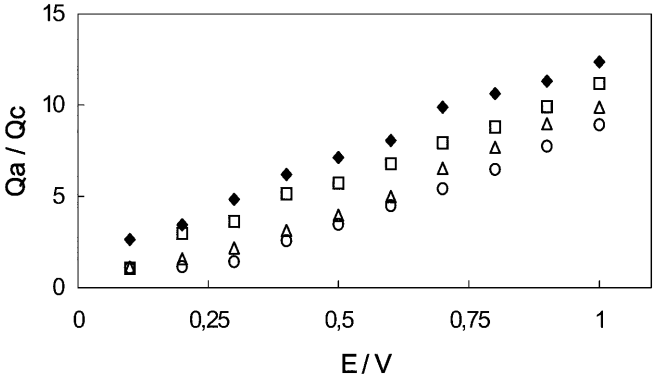

Fig. 6 Dependence of Q_a/Q_c ratio on anodic end point potential in acetic acid/acetate buffer, pH 4.5, at 298 K and sweep rate 20 mV s^{-1}: (◆) polished electrode, (❑) Py21, (Δ) Py2125 and (○) Py25

by the pyrite oxidation increases from approximately 20% to 80% as the sulfur production decreases at the same rate (Fig. 7c). This potential region ($E_{oc} < E < 0.6$ V) is usually associated with pyrite passivation, owing to the presence of a film of elemental sulfur formed on the electrode surface. The results shown in Fig. 7b and Fig. 7c suggest that elemental sulfur is not accumulating on the mineral surface to inhibit the dissolution process.

The relative quantity of sulfate produced by all electrodes reaches a maximum value at $E_{\lambda a} \geq 0.6$ V (Fig. 7b). At high overpotentials, the oxidation of pyrite seems to be independent of the pre-history of the electrode. The percentage of S (Fig. 7c) decreases as a function of $E_{\lambda a}$ and reaches a minimum value at potentials more positive than 0.5 V. This result agrees with others [18, 19], which report potentials at which the formation of sulfur becomes negligible in relation to the quantity of sulfate formed. Moreover, the production of elemental sulfur seems to be limited to 50%, which is consistent with the idea that sulfur and sulfate are formed from the decomposition of a single intermediate, such as thiosulfate [19, 20, 21]. The formation of polysulfides was not considered for two main reasons: (1) the thiosulfate path dominates in acidic electrolytes and only in solutions with higher pH does the stability of polysulfides increase, allowing the polysulfide path to be favored [22]; (2) without chemical etching, which causes an enrichment of sulfur compounds at the surface, favoring the polysulfide oxidation [23], pyrite surfaces are not expected to form polysulfides at potentials more negative than 1.2 V [8].

The very limited oxidation rate of the mineral at potentials more negative than 0.6 V was attributed to its

semiconducting properties [18]. The first step of the reaction mechanism may be interactions of OH^- ions with the iron sites [19] or the adsorption of H^+ at a Lewis base site on the mineral surface, i.e. at a sulfur ion [18]. The intermediate, in both cases, would be $S_2O_3^{2-}$, which either is oxidized to sulfate or decomposes to produce elemental sulfur and bisulfite. Previous authors [18, 19] relate the first step of the reaction to being highly dependent on the semiconducting properties of the mineral.

The results showed herein confirm that the oxidation of pyrite in aqueous medium takes place through thio intermediates, owing to the fact that, in addition to sulfate ions, elemental sulfur was generated during the dissolution process. The incoming OH^- [19] or H^+ [18] ions to the mineral surface determines the possibility of reaction, which is favored by the smaller grain size. As relative quantities were used to calculate the yield of oxidation products, it is clear that the increase in the surface area is not the only reason for the increase in the reaction rate.

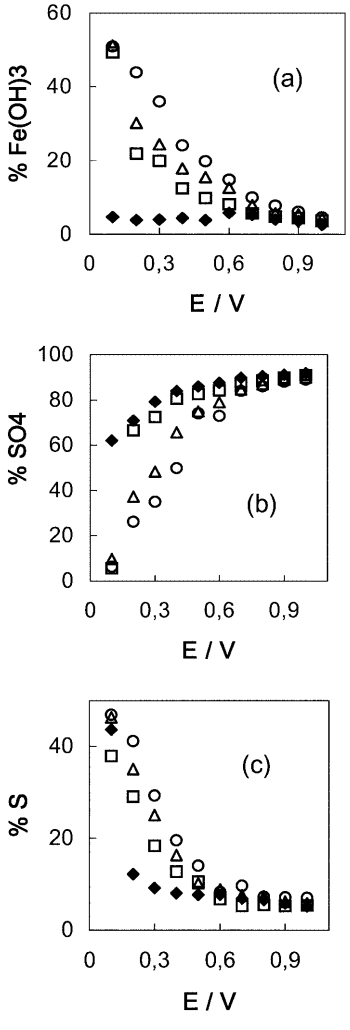

Fig. 7 Dependence of the relative quantities of iron hydroxide (**a**), sulfate (**b**) and sulfur (**c**) from pyrite oxidation on anodic end point potential in acetic acid/acetate buffer, pH 4.5, at 298 K and sweep rate 20 mV s^{-1}: (◆) polished electrode, (❑) Py21, (Δ) Py2125 and (○) Py25

Thermal behavior

The TG curves show that the mineral is thermostable until nearly 450 °C and a two-stage weight loss is observed (Fig. 8). The main oxidation reaction occurs in the temperature range between 490 and 550 °C. The TG curves associated with the samples Py25 and Py2125 present an inflection, indicating the occurrence of two processes. Between 550 and 700 °C a little weight gain is observed in all cases and may be due to sulfate formation. According to several authors [23, 24, 25, 26, 27, 28], the first weight loss in the TG curves corresponds to the oxidation of pyrite to hematite, whilst the second weight loss is associated with the formation of an iron sulfate phase. The weight loss calculations are based on the total weight loss between 400 and 900 °C, being the 100% conversion of the pyrite to hematite.

In order to establish the reaction sequence, the experiments were stopped and the residue analyzed by infrared spectroscopy. The residue obtained at 550 °C (Fig. 9a) was composed of hematite and iron sulfate, which is proposed as an intermediate in the pyrite oxidation by various authors [29, 30, 31]. The residue obtained at 900 °C (Fig. 9b) in all cases shows the presence of hematite (Fe_2O_3), which confirms that the oxidation reaction is complete at this temperature. The inserts in Fig. 9a and Fig. 9b show the IR spectra of $FeSO_4$ and hematite, which are in good agreement with published results [32].

The effect of particle size on the TG-DTG results is presented in Fig. 10 for pyrite heated at 10 °C min^{-1} in an air flow of 10 mL min^{-1}. The particle size effect is better observed in the DTG curves. For the largest particle size, Py25, the DTG record shows a double peaking effect around 400 °C (Fig. 10c). For the intermediate particle size, Py2125, the second peak is less

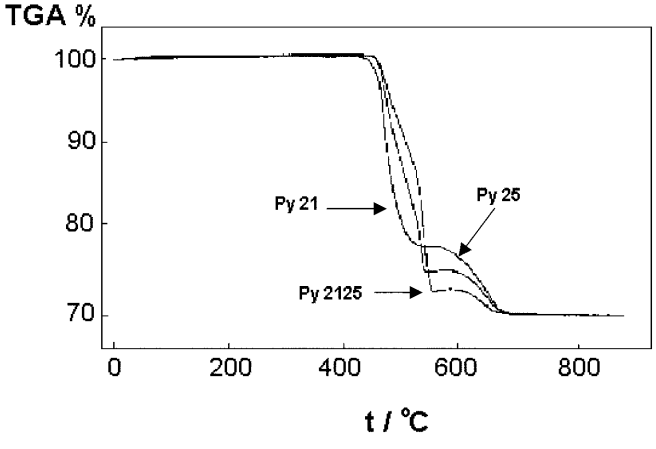

Fig. 8 TG curves for pyrite treated in an air atmosphere at a heating rate of 10 °C min^{-1}

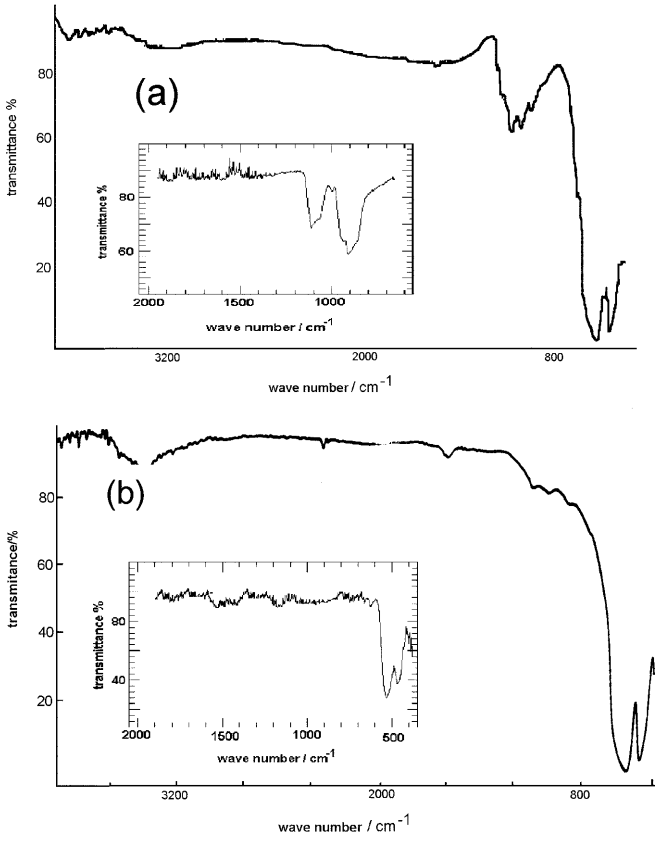

Fig. 9 Infrared spectra of Py2125 sample heated to **a** 550 °C with *insert* of $FeSO_4$ spectrum and **b** 900 °C with *insert* of hematite spectrum

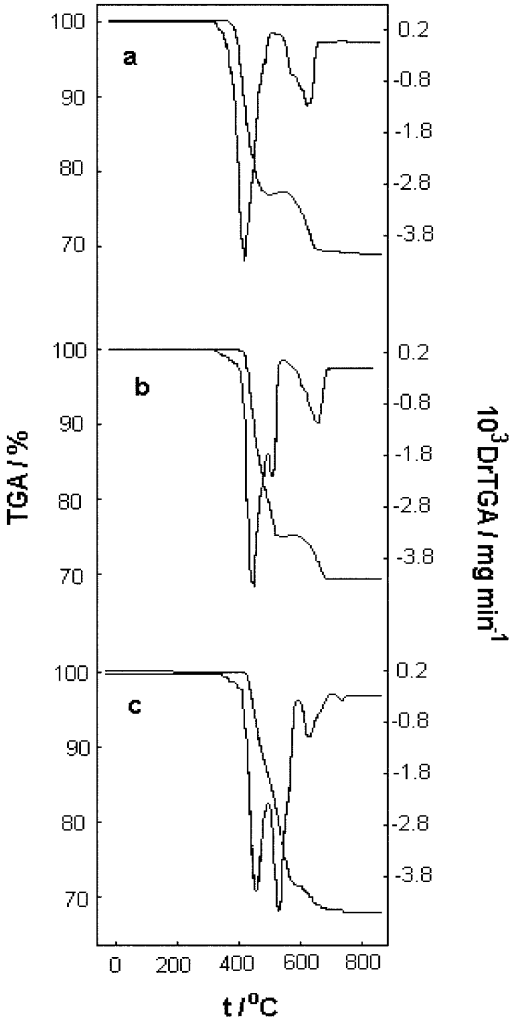

Fig. 10 TG-DTG curves for pyrite treated in an air atmosphere at a heating rate of 10°C min^{-1} and flow rate of 10 mL min^{-1}: **a** Py21, **b** Py2125 and **c** Py25

intense (Fig. 10b) and finally, with the Py21 particles, just one peak is recorded in this temperature region (Fig. 10a). Similar behavior was observed with air flow rates of 40 mL min^{-1} and 80 mL min^{-1}. The results at 80 °C min^{-1} show similar trends, demonstrating that the effect is reproducible and is not affected by the differing heating or air flow rates. These modifications in the DTG curves are significant enough to suggest that the oxidative transformation may be affected by the particle size. The effect of particle size is due to two major factors. First, the smaller is the particle, the greater will be the surface area to mass ratio. Thus, Py21 has a larger interfacial area available for oxidation and may react at a faster rate. Second, less time is required to completely oxidize a small particle, as the oxygen diffusion into the Py21 particles is faster than that for the larger particles. According to Dunn et al. [28], oxidation of pyrite occurs via a shrinking core mechanism, with the increasing movement of the reaction front towards the center of the particles. The oxide/sulfate coating formed is protective and prevents the oxygen diffusion process. If sufficient time is allowed, small particles will be completely oxidized by this mechanism. There are two oxidative reactions: the conversion of pyrite to hematite, causing the first weight loss, and the formation of sulfate. Direct oxidation to hematite is encouraged by a small particle size and faster heating rates, whilst sulfate formation is favored by slow heating rates and an oxygen atmosphere [28].

The increase of the air flow rate from 40 mL min^{-1} to 80 mL min^{-1} is shown in Fig. 11. For the larger particle sizes, Py25 and Py2125, the interference of the air flux is noted between 490 and 550 °C, inhibiting the first step of the weight loss and favoring the second one.

The double peaking is probably due to two competing reactions occurring at this temperature range (Eqs. 7 and 8):

$$FeS_2 + 3O_2 \rightarrow FeSO_4 + SO_2 \quad (7)$$

$$2FeS_2 + 5.5O_2 \rightarrow Fe_2O_3 + 4SO_2 \quad (8)$$

It is known that a platinum crucible catalyses SO_2 to SO_3 [27, 28]. Thus, at temperatures higher than 550 °C, the small weight gain which is observed may be attributed to the formation of $FeSO_4$ (Eq. 9):

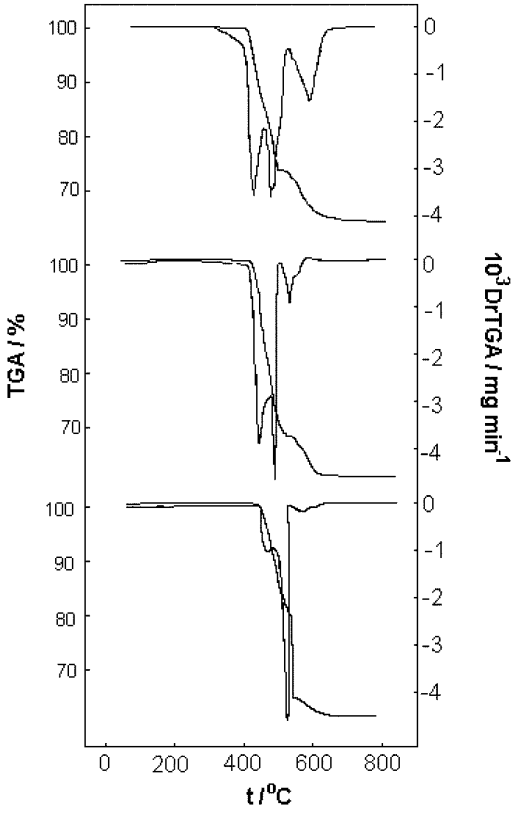

Fig. 11 TG-DTG curves for Py2125 treated in an air atmosphere at a heating rate of 10°C min^{-1} and a flow rate of: (*top*) 10 mL min^{-1}, (*middle*) 40 mL min^{-1} and (*bottom*) 80 mL min^{-1}

$$Fe_2O_3 + SO_2 + SO_3 \rightarrow 2FeSO_4 \quad (9)$$

The increase of the air flow rate (Fig. 11) may favor the process represented by Eq. 7; more $FeSO_4$ than Fe_2O_3 is produced and consequently the weight gain between 550 and 600 °C is smaller. The same effect is observed when the particle size is decreased (Fig. 10). Increasing the grain size increases the time to completely oxidize the particles and allows reaction 7 to occur. However, maintaining the grain size and increasing the air flux results in an oxygen input which favors sulfate production. For particles less than 210 μm in size, the first weight loss does not present the double peaking observed in the other samples, and increasing the air flow rate does not affect significantly the oxidation.

Electrochemical versus thermal behavior

The data obtained by thermal analysis and voltammetry show that the pyrite oxidation presents similar trends when examined by these two methods. In aqueous medium, the oxidation occurs only when the potential reaches values more positive than 0.6 V. In air, there is a minimum temperature below which the oxidation reactions do not occur. Thus, it may be suggested that the very restricted oxidation rate of the mineral in air should also be attributed to its semiconducting properties.

The pyrite used in this study is an n-type semiconductor. With increasing temperature, electrons are thermally excited and two charge carriers are generated: an electron in the conduction band and a hole in the valence band. Egglestone et al. [33] studied the mineral oxidation in air and proposed a mechanism where Fe(III) accumulates on the surface and may act as a conduit between pyrite and dissolved O_2. In the case of thermal analysis, the oxygen molecules in the crucible have sufficient affinity to capture an electron from the conduction band, which may lead to the formation of O_2^- and O^- species, the second one dominating at high temperatures [34]. However, the techniques used here do not permit us to infer if this electron comes from an oxidized site or from pyrite itself. The charged adsorbate, O^-, can locate itself at the Fe sites:

$$FeS_2 + O^- + h^+ \rightarrow Fe\ O\ S_2 \quad (10)$$

The O^- species spread along the surface, leading to the formation of hematite:

$$2FeS_2 + 11O^- + 11h^+ \rightarrow Fe_2O_3 + 4SO_2 \quad (11)$$

These steps resemble that proposed by Mishra and Osseo-Asare [19] for the oxidation of pyrite in aqueous medium. Hence, it may be suggested that the charged adsorbate may be rearranged on the pyrite surface, moving in direction to the S_2^{2-} sites:

$$Fe\ O^-S_2 \rightarrow Fe\ S_2O^- \quad (12)$$

leading to the formation of iron sulfate:

$$Fe\ S_2O^- + 5O^- + 6h^+ \rightarrow FeSO_4 + SO_2 \quad (13)$$

Corresponding to the results obtained from cyclic voltammetry, before the main weight loss (between 490 and 550 °C) the samples even in a large excess of air required at least 40 min to initiate the oxidation process (Fig. 8). This would suggest that the dissociation of the pyrite has taken place, while the extracted elemental sulfur remains on the surface of the mineral particle [35]. However, comparison with the results obtained from electrochemical methods suggests the rate-controlling factor may be the interaction between the surface and the oxygen ions in the crucible. Thus, it is assumed that oxygen diffusion towards and into the pyrite particle is the principal cause of the oxidation reaction. The arrival of O^- species at the mineral surface determines the possibility of reaction, which may be favored by the smaller grain size. The time required for the charged adsorbate to reach the S_2^{2-} sites would determine the quantity of intermediate to be formed.

At potentials more positive than 0.6 V or at temperatures higher than 490 °C, it is clear that the oxidation of the mineral takes place through sulfoxy intermediates. The quantity of sulfate obtained will depend on the experimental conditions. In aqueous

media, the ratio SO_4^{2-}/S varies with the applied potential and the pH of the solution. In absence of water, sulfate formation is influenced by the air flow rate and the temperature.

Conclusions

The comparison between the results obtained from the two methods suggests that the interaction of the mineral surface and the oxygen species (O^- or OH^-) is the rate-controlling step of the oxidation either in air or in aqueous medium. Thus, the smaller the grain sizes, the faster will be the oxidation. Moreover, as the dimensions of the particles facilitate the contact of the oxygen species, the occurrence of parallel reactions is disfavored.

The results showed, also, that the greater reactivity of the small particles is due not only to an increase in the surface area. The number of active sites usually gives the reactivity of the mineral electrodes. Apart from additional influences disregarded in this discussion, this depends on the number of active surface sites, an intensive variable. This parameter is affected by the operating process; the more efficient the pretreatment used, the more active centers are formed. Thus, the higher will be the reactivity of the ground mineral and the extent of any reaction on its surface. Hence, the FeS_2 polished electrodes dissolve faster than ground ones. In the same manner, the more particles that are ground, the more active sites will be available.

Acknowledgements Financial support from Fundação de Amparo à Pesquisa do Estado de São Paulo, FAPESP, Proj. 95/9333-2, is gratefully recognized. Special thanks to Professors A.V. Santos and J.R. Matos, for assistance with the thermal analysis and for valuable comments.

References

1. Peters E, Majima H (1968) Can Metall Q 7:11
2. Lux L, Gálová M, Hezelová M, Markusová K (1999) J Solid State Electrochem 3:288
3. Lamache M (1979) Electrochim Acta 24:79
4. Adriamanana A, Lamache M, Bauer D (1984) Electrochim Acta 29:1054
5. Karthe S, Szargan R, Suoninen E (1993) Appl Surf Sci 72:157
6. Ramprakash Y, Koch DFA, Woods R (1991) J Appl Electrochem 21:531
7. Hamilton C, Woods R (1981) J Electroanal Chem 118:327
8. Giannetti BF, Bonilla SH, Zinola CF, Rabóczkay T (2001) Hydrometallurgy 60:41
9. Leclerc O, Bauer D (1990) Analusis 18:278
10. Buckley NA, Woods R (1987) Appl Surf Sci 27:437
11. Mitchel D, Woods R (1978) Aust J Chem 3:27
12. Encinas P, Lorenzo L, Tascón ML, Vásquez MD, Sánchez-Batanero P (1994) J Electroanal Chem 371:161
13. Mouhandess MT, Chassagneux F, Vittori O (1982) J Electroanal Chem 131:367
14. Sharara ZZ, Vittori O (1984) Electrochim Acta 29:1689
15. Flatt JR, Woods R (1995) J Appl Electrochem 25:852
16. Antonijevic MM, Dimitrijevic M, Janjovic Z (1997) Hydrometallurgy 46:71.
17. Dimitrijevic M, Antonijevic MM, Janjovic Z (1996) Hydrometallurgy 42:377
18. Kelsall GH, Yin Q, Vaugham DJ, England KER, Brandon NP (1999) J Electroanal Chem 471:116
19. Mishra KK, Osseo-Asare K (1988) J Electrochem Soc 135:2502
20. Biegler T, Swift DA (1970) Electrochim Acta 24:412
21. Jonhston F, Mcamish LJ (1973) Colloid Interface Sci 42:112
22. Mycroft JR, Bancroft GM, McIntyre NS, Lorimer JW, Hill IR (1990) J Electroanal Chem 292:139
23. Ennaoui A, Fietcher S, Jaegermann W, Tributsch H (1986) J Electrochem Soc 133:97
24. Jorgensen FRA, Moyle FJ (1981) Met Trans B 12:9
25. Paulik F, Paulik J, Arnold M (1986) J Therm Anal 31:145
26. Dunn JG, De GC, Fernandez PG (1988) Thermochim Acta 135:267
27. Dunn JG, De GC, O'Connor BH (1989) Thermochim Acta 155:135
28. Dunn JG, De GC, O'Connor BH (1989) Thermochim Acta 145:115
29. Paulik F, Paulik J, Arnold M (1982) J Therm Anal 25:313
30. Jorgensen FRA, Moyle FJ (1982) J Therm Anal 25:473
31. Kennedy T, Sturman BT (1975) J Therm Anal 8:329
32. Nyquist RA, Kagel RO (1997) Handbook of infrared and Raman spectra of inorganic compounds and organic salts. Academic Press, New York
33. Egglestone CM, Ehrhardt JJ, Stumm W (1996) Am Mineral 81:1036
34. Morrison SR (1990) The chemical physics of surfaces. Plenum Press, New York
35. Zikovic ZD, Molosavljevic N, Sestak J (1990) Thermochim Acta 157:215